Magnetic proximity coupling to Cr-doped Sb_2Te_3 thin films

L. B. Duffy,[1,2] A. I. Figueroa,[3] Ł. Gładczuk,[1,3] N.-J. Steinke,[2] K. Kummer,[4] G. van der Laan,[3] and T. Hesjedal[1,*]

[1]*Department of Physics, Clarendon Laboratory, University of Oxford, Oxford, OX1 3PU, United Kingdom*

[2]*ISIS, STFC, Rutherford Appleton Lab, Didcot, OX11 0QX, United Kingdom*

[3]*Magnetic Spectroscopy Group, Diamond Light Source, Didcot, OX11 0DE, United Kingdom*

[4]*European Synchrotron Radiation Facility, BP 220, 38043 Grenoble Cedex, France*

(Received 20 March 2017; revised manuscript received 9 May 2017; published 19 June 2017)

Using soft x-ray absorption spectroscopy we determined the chemical and magnetic properties of the magnetic topological insulator (MTI) Cr:Sb_2Te_3. X-ray magnetic circular dichroism (XMCD) at the Cr $L_{2,3}$, Te $M_{4,5}$, and Sb $M_{4,5}$ edges shows that the Te $5p$ moment is aligned antiparallel to both the Cr $3d$ and Sb $5p$ moments, which is characteristic for carrier-mediated ferromagnetic coupling. Comparison of the Cr $L_{2,3}$ spectra with multiplet calculations indicates a hybridized Cr state, consistent with the carrier-mediated coupling scenario. We studied the enhancement of the Curie temperature, T_C, of the MTI thin film through the magnetic proximity effect. Arrott plots, measured using the Cr L_3 XMCD, show a $T_C \approx 87$ K for the as-cleaved film. After deposition of a thin layer of ferromagnetic Co onto the surface, the T_C increases to ~93 K, while the Co and Cr moments are parallel. This increase in T_C is unexpectedly small compared to similar systems reported earlier. The XMCD spectra demonstrate that the Co/MTI interface remains intact, i.e., no reaction between Co and the MTI takes place. Our results are a useful starting point for refining the physical models of Cr-doped Sb_2Te_3, which is required for making use of them in device applications.

DOI: 10.1103/PhysRevB.95.224422

I. INTRODUCTION

Topological insulators (TIs) are of key significance due to their exotic physical nature and promising electronic properties [1,2], which could lead to advancements in low-power consumption devices for a range of applications [3]. Three-dimensional TIs have gapless topological surface states protected by time-reversal symmetry (TRS), which take the form of linearly dispersed Dirac cones with spin-momentum locking [4]. These states are resilient to weak disorder or impurities [5], however, by breaking the TRS a gap can be opened at the Dirac point. This has led to both the prediction and observation of exotic quantum phenomena. Most notably the quantum anomalous Hall effect (QAHE), a fundamental quantum transport phenomenon, has been observed [6]. It is thought that this effect will be the key to unlocking major advancements in dissipationless quantum electronics [7]. The breaking of TRS can be achieved through two different methods, which result in the application of a magnetic field: via proximity to a ferromagnetic layer, or by achieving magnetic long-range order in the TI by doping (e.g., with Fe [8], Mn [9], or Cr [10]). Magnetically doped TIs (MTIs) have exhibited giant spin-orbit torque, tunable via the use of an electric field, demonstrating potential applications for spintronics [11].

V- and Cr-doping of $(Sb,Bi)_2(Se,Te)_3$ have proven to be some of the most promising ways of producing MTIs [12–14], allowing for the experimental verification of the QAHE [15]. For Cr-doped Bi_2Se_3, it has previously been demonstrated that the ferromagnetic transition temperature, T_C, can be enhanced from 7–19 K through the deposition of a Co layer onto the surface of the MTI [16]. Despite this more than doubled T_C it is still well below accessible temperatures for practical applications. On the other hand, magnetic ordering at much higher temperatures has been reported for $Cr_xSb_{2-x}Te_3$ thin films, such as 125 K for $x = 0.42$ [14] and 190 K for $x = 0.59$, following a nearly linear increase with Cr doping [17].

The $3d$ states of the transition metal impurities play an important role in MTIs by providing additional mechanisms of ferromagnetic coupling [18,19], although these mechanisms have yet to be experimentally confirmed. Recently, it has become clear that the proposed Van Vleck mechanism [20,21] is not sufficient to explain the more complex coupling mechanism in these systems [22].

Recently, we reported the structural, electronic, and magnetic investigation of molecular beam epitaxy (MBE)-grown $Cr_xSb_{2-x}Te_3$ thin films ($x = 0.15$, 0.26, 0.42) using x-ray diffraction (XRD), atomic force microscopy, superconducting quantum interference device (SQUID) magnetometry, magnetotransport, and polarized neutron reflectometry, showing these materials retain good crystalline order [14]. X-ray magnetic circular dichroism (XMCD) measurements on Cr-doped $(Sb,Bi)_2Te_3$ were recently reported by Ye *et al.* [18]. In the current paper, we report on the magnetic proximity coupling of these materials. We investigate the magnetic properties of *in situ* cleaved $Cr_{0.32}Sb_{1.68}Te_3$ thin films before and after deposition of a Co overlayer using XMCD. The isothermal magnetization curves are measured by XMCD as a function of field in order to produce Arrott plots [23], revealing the T_C of the sample both before and after deposition. It is found that—unlike other systems—the proximity effect between the Co layer and MTI layer is weaker than might have been expected. It would be important to understand why this is the case in order to fully utilize this method of enhancing the properties of MTIs for device applications.

*thorsten.hesjedal@physics.ox.ac.uk

II. EXPERIMENTAL

MBE was used to grow Cr-doped Sb_2Te_3 thin films on *c*-plane sapphire substrates, with a typical film thickness of ∼40 nm. For the Sb_2Te_3 growth, a Sb:Te flux ratio of 1:10 was maintained. Cr was provided out of a high-temperature effusion cell, while maintaining a flux ratio of (Sb+Cr):Te of 1:10. The thin film deposition took place at a substrate temperature of 250°C. A detailed description of the growth procedure can be found in Ref. [14].

Structural and magnetic characterization was carried out using XRD and SQUID magnetometry (for details see Ref. [14]). Out-of-plane XRD measurements show that the films are free from secondary phases, such as chromium tellurides, which have T_Cs between 180 and 340 K [24]. The shift of the Sb_2Te_3 peak positions to higher angles is consistent with the Cr atoms substituting Sb in the crystal structure. This is due to a reduction in the Cr-Te bond length, when compared to the Sb-Te bonds, since Cr has a smaller ionic radius [14]. SQUID magnetometry demonstrates that the samples are ferromagnetic with a coercive field of ∼50 mT at 5 K, and with an out-of-plane easy axis (saturation field = 200 mT) and an in-plane hard axis (saturation field = 2 T). The T_C of the film, defined by the minimum of the first derivative of the temperature-dependent magnetization [14], is ∼72 K. However, the accuracy of the SQUID result is quite low, owing to the large background signal. The method of derivative-based T_C is systematically underestimating its value, see, e.g., Ref. [25]. The shift in the Sb_2Te_3 peaks in XRD, and the minimum of the first derivative of the temperature-dependent magnetization from SQUID, also give an indication of the doping concentration of the film. By comparing these sets of data to identical samples with varying Cr abundance, which have had their concentration measured accurately using Rutherford back-scattering spectrometry a Cr concentration of ∼6.4 at.% was estimated.

The Cr-doped Sb_2Te_3 sample was characterized using x-ray absorption near edge structure (XANES) and extended x-ray absorption fine structure measurements (EXAFS) at the Cr *K* edge on beam line B18 at the Diamond Light Source [26]. The XANES results show that the energy position of the edge jump is the same as for the reference sample CrSe, revealing a similar local electronic environment, in which the Cr is nominally divalent. Analysis of the EXAFS results show Cr-Te distances with coordination number $N = 6$ and radial distance $R = 2.776$ Å. This clearly demonstrates that the Cr enters substitutionally into the Sb sites with octahedral symmetry. This is consistent with the fact that after doping the XRD does not show a lattice expansion in the *c* direction, which would occur if the Cr enters into the van der Waals gap. The crystal structure of the Cr-doped Sb_2Te_3 is shown in Fig. 1, where the substitutional Cr in an octahedral environment is surrounded by six nearest-neighbor Te atoms.

XMCD measurements were performed on beam line ID32 at the European Synchrotron Radiation Facility (ESRF) in Grenoble. X-ray absorption spectroscopy (XAS) was measured at the Co and Cr $L_{2,3}$ and Sb $M_{4,5}$ edges in total-electron-yield (TEY) mode, giving a surface sensitive probing depth of 3–5 nm [27]. The samples were cleaved in ultrahigh vacuum to ensure a pristine surface. The samples were *in situ*

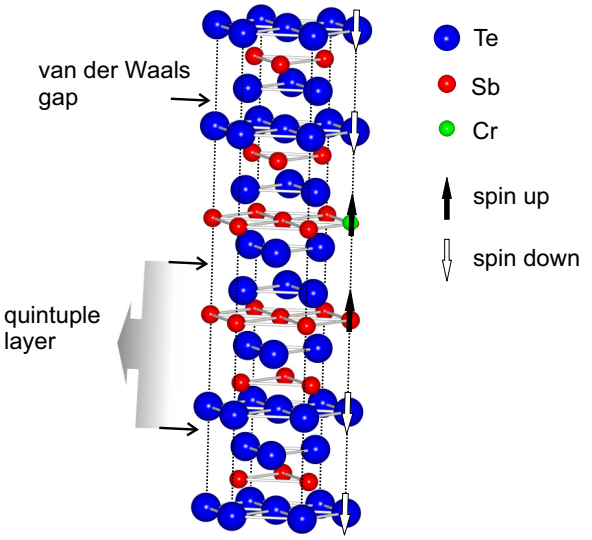

FIG. 1. Crystal structure of Cr-doped Sb_2Te_3 showing the quintuple layers (Te-Sb-Te-Sb-Te), which are separated by the van der Waals gap (indicated by arrows). The Cr dopant is shown substitutional on a Sb site, which is surrounded by six Te atoms. The relative spin orientations can be summarized as (Cr,Sb)↑-(Te)↓ and are indicated by the arrows in the figure.

magnetized with an initially applied field of 1 T. The XMCD was obtained by taking the difference between XAS spectra with the helicity vector antiparallel and parallel to the initially applied magnetic field, respectively. In the case that a field was applied during the measurements both the helicity and the field were reversed to check the consistency of the XMCD signal [27]. Measurements were carried out with the sample both normal to the incident x rays and at an angle of 54.7° (magic angle) to accommodate for the perpendicular magnetization directions of the Co and the MTI. In uniaxial symmetry, as for thin films, the anisotropic contribution in the spin and orbital moments disappears at the magic angle [28,29].

After performing measurements on the pristine sample, Co was evaporated from an e-beam evaporator situated inside the XAS measurement chamber (base pressure $<1 \times 10^{-9}$ Torr) at $T < 10$ K. This low-temperature evaporation prevents clustering of the Co atoms [30]. The Co layer needs to be magnetic at remanence, which requires a thickness ⩾3 nm, as determined by the material's characteristic exchange length. On the other hand, the Co layer needs to be thin enough that it does not suppress too much the TEY signal from the underlying MTI layer. To ensure the Co layer was magnetic, XMCD measurements were carried out periodically during the different stages of evaporation by flipping the x-ray helicity. The XAS and XMCD lineshape and intensity were recorded during this process at both the Co and Cr $L_{2,3}$ edges to ensure they remained consistent with clean Cr and a subsequently grown clean ∼3-nm-thick Co film.

III. RESULTS

A. XAS and XMCD spectra

Figure 2(a) shows the Cr $L_{2,3}$ XAS and XMCD measured in TEY for the *in situ* cleaved $Cr_xSb_{2-x}Te_3$ sample ($x = 0.32$).

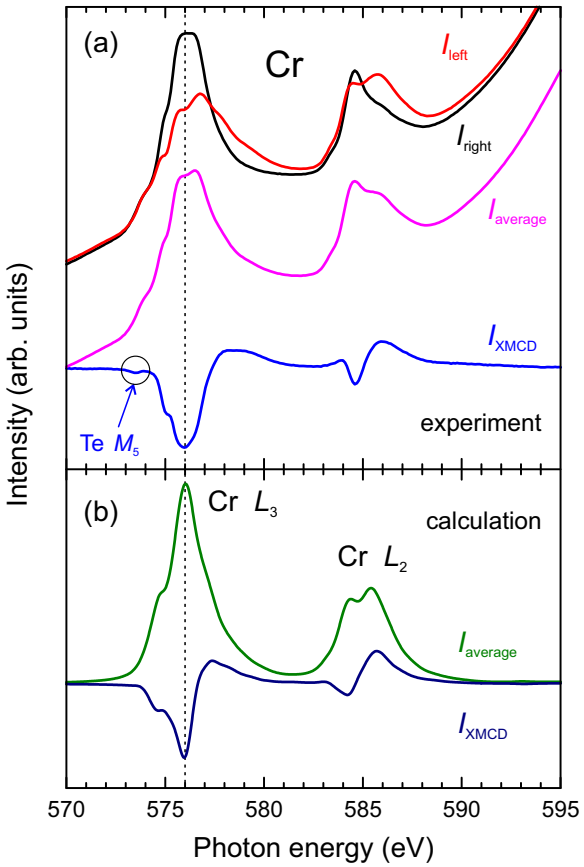

FIG. 2. Cr $L_{2,3}$ XAS and XMCD of an *in situ* cleaved $Cr_{0.32}Sb_{1.68}Te_3$ film measured in zero field at 10 K with normal incidence of the incident x rays. An initial field of 1 T was applied before the measurement. (a) Experimental spectra for left- and right-circularly polarized x rays, together with the average and difference (XMCD) signals. The small negative peak at 573.4 eV in the XMCD (marked by a circle) originates from the Te M_5 edge. (b) Calculated average XAS and XMCD spectra for a hybridized Cr ground state with 70% d^4 and 30% d^3 character.

The XAS of the Cr L_3 shows mainly a double peak structure, where the first peak (marked by a dashed vertical line) is much more dichroic than the second peak at a ∼0.5 eV higher energy. In contrast, for bulk $Cr_xBi_{2-x}Se_3$, as reported in Refs. [13,16], this second peak is much lower in intensity. It is important to note that this second peak is not due to oxidation. As was shown in Ref. [13], the main contribution from the surface oxide is at 1.5 eV higher energy, coinciding with the reference spectrum for Cr_2O_3. The XMCD line shape of $Cr_xSb_{2-x}Te_3$ is very similar to that reported for bulk $Cr_xBi_{2-x}Se_3$, including the small shoulder at 0.6 eV below the L_3 maximum and the characteristic sharp negative peak in the L_2 edge at 584.6 eV (see Refs. [13,16]). Note that despite the negative dip, the overall intensity of the Cr L_2 is still positive, and thus opposite to the L_3 edge, as imposed by the $2p$ spin-orbit coupling [31].

The Cr $L_{2,3}$ absorption largely coincides with the Te $M_{4,5}$ absorption edges. This is the main reason for the strongly sloping background of the XAS, which almost completely cancels out in the XMCD difference spectrum—except for a small negative peak at 573.4 eV exposing the Te M_5 [encircled in Fig. 2(a)], with the same sign as the Cr L_3 XMCD. The Te M_5 XMCD changes sign for opposite field direction (keeping the helicity fixed) and also changes sign for opposite helicity (keeping the field fixed), just as the Cr L_3 XMCD.

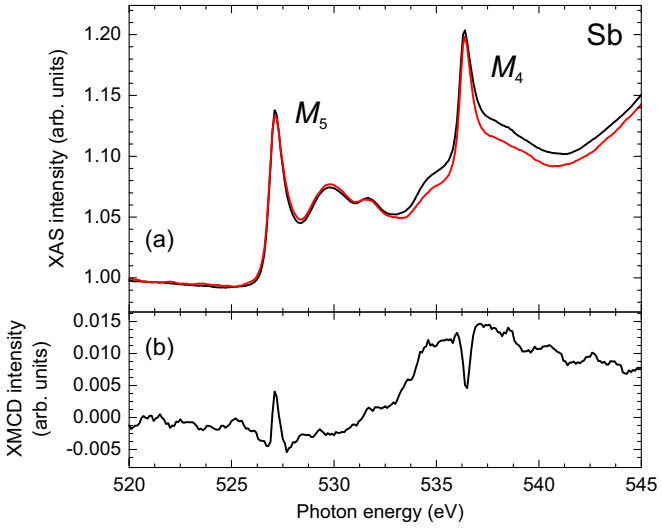

FIG. 3. *In situ* cleaved $Cr_{0.32}Sb_{0.68}Te_3$ film measured at the Sb $M_{4,5}$ edges ($3d \rightarrow 5p$) in 8 T field at 3 K. (a) XAS measured using left-circularly (black curve) and right-circularly (red curve) polarized x rays and (b) corresponding XMCD.

The Sb $M_{4,5}$ XAS and XMCD spectra are presented in Fig. 3, which shows that the leading sharp peaks are dichroic, evidencing an induced magnetic moment on the Sb sites. The Sb M_5 XMCD has opposite sign compared to the Cr L_3 XMCD.

Figures 4(a) and 4(b) show the Co $L_{2,3}$ XAS and XMCD spectra measured at 10 K after the deposition of a thin Co layer onto the cleaved $Cr_xSb_{2-x}Te_3$ sample. Clearly, the XMCD measured at remanence by switching the x-ray helicity shows that the Co layer is ferromagnetic with a moment aligned parallel to that of the Cr dopants. Figure 4(c) shows the Cr $L_{2,3}$ XMCD taken before and after Co deposition. The spectra are almost identical. After deposition a small reduction is visible for the low-energy shoulder of the XMCD at 575.1 eV [see inset in Fig. 4(c)]. The same effect was also observed for $Cr_xBi_{2-x}Se_3$ [16], suggesting a more general origin. We ascribe this reduction to a small increase in delocalization of the Cr $3d$ states after Co deposition. Overall, Fig. 4(c) clearly demonstrates that there is no significant interfacial reaction between the MTI and Co layer, and that the chemical state of the Cr in the MTI is not altered. It excludes that there is any significant Cr diffusion into the Co film, or vice versa. Furthermore, the valence state of the Cr dopants remains the same, since the presence of Cr^{3+} would give rise to a peak structure at ∼1.5 eV higher photon energy.

B. Arrott plots

For the practical determination of the Curie temperature, T_C, of a material, one is confronted with several issues. For one, it has to be ensured that the sample is in a single domain state. This usually requires the application of a magnetic field, which

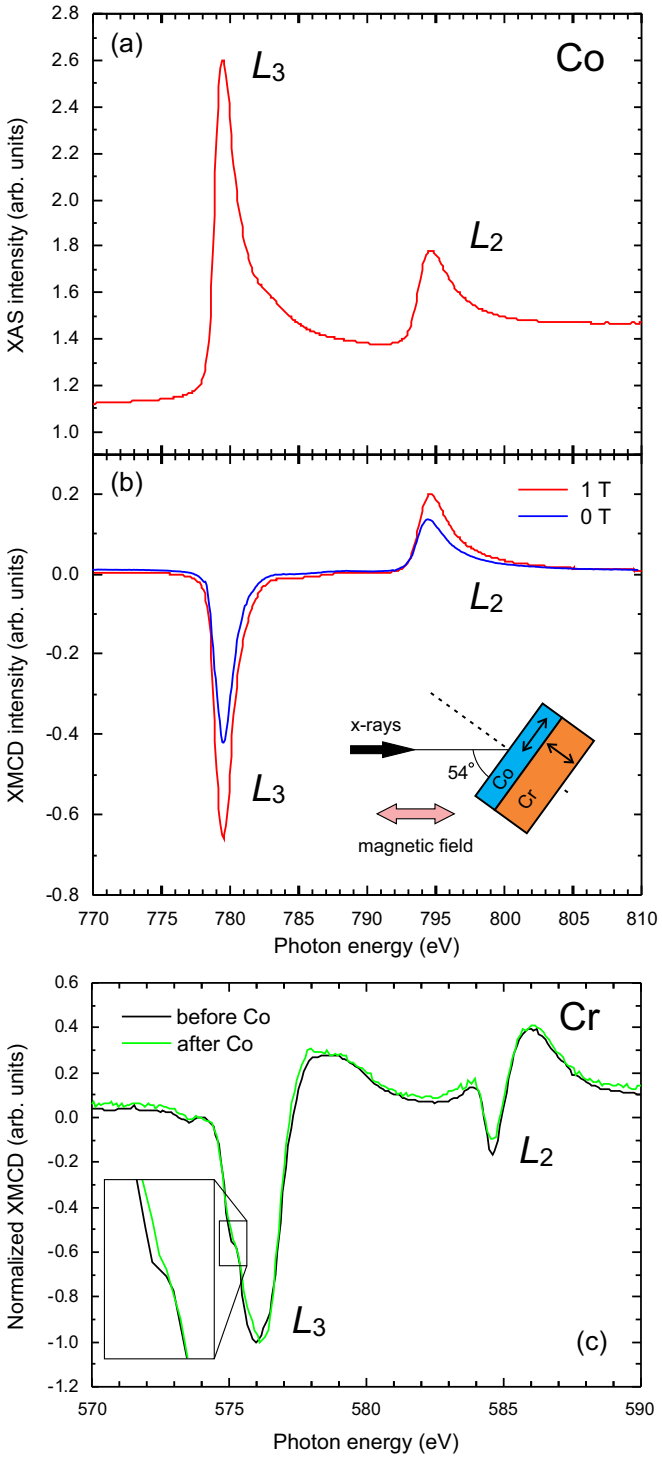

FIG. 4. *In situ* cleaved $Cr_{0.32}Sb_{1.68}Te_3$ film after Co deposition. (a) XAS and (b) XMCD measured at the Co $L_{2,3}$ edge in an applied magnetic field of 1 T (red) and at remanence (blue), at a temperature of 10 K, and with an incident angle of the x rays of 54°, as shown by the geometry in the inset. (c) Comparison of the Cr $L_{2,3}$ XMCD signals before (black line) and after (green line) Co deposition. The inset shows a blow up of the small shoulder at 575.1 eV.

in turn affects the (apparent) T_C of the sample. Furthermore, if the coercive field is particularly small, it is difficult to observe the closure of the hysteresis loop at T_C. The most reliable method for determining T_C of a ferromagnet is offered by the Arrott-Noakes criterion [32], which minimizes the contribution arising from domains and magnetic anisotropy. In the case of a conventional second-order ferromagnetic transition, the Arrott plot should show positively sloped straight lines if the magnetic field is high enough so that possible domain or stray-field effects become negligible.

The Arrott-Noakes equation is given as [32]

$$\left(\frac{H}{M}\right)^{1/\gamma} = \frac{T - T_C}{T_1} + \left(\frac{M}{M_1}\right)^{1/\beta}, \tag{1}$$

where M is the magnetization, H is the applied field, T is the temperature, and T_1 and M_1 are material dependent parameters. In the mean-field theory, $\beta = 0.5$ and $\gamma = 1$, in which case Eq. (1) simplifies to

$$M^2 = A\frac{H}{M} + B\,(T - T_C), \tag{2}$$

with $A = (M_1)^2$ and $B = -(M_1)^2/T_1$. An Arrott plot consists of a set of isotherms for M^2 vs H/M. In the high-field region, these isotherms are expected to be parallel straight lines, whereas disorder in a system can lead to a bending towards lower applied fields [33,34].

The Arrott plot for the as-cleaved sample is depicted in Fig. 5(a), where M is obtained by using the background-corrected Cr L_3 XMCD asymmetry. Figure 5(b) shows the Arrott plot, produced in the same manner, for this sample after the Co deposition. For all isotherms the intercepts with the M^2 axis were determined by fitting parallel straight lines with the same gradient to the high-field region [dotted lines in Figs. 5(a) and 5(b)]. The intercept is positive for $T < T_C$ and negative for $T > T_C$. Equation (2) means that T_C is equal to that temperature for which the isotherm passes through the origin, i.e., where the M^2 intercept is zero. Figure 5(c) shows the M^2 intercepts gathered for the sample with and without Co deposition, from which we can obtain the zero crossings. For the as-cleaved sample, $T_C \approx 87$ K, whereas after the Co deposition the T_C rises to ~93 K, which represents a rather modest increase.

IV. DISCUSSION

A. Chemical state

If a Cr dopant enters into the lattice interstitially, or into the van der Waals gap, i.e., if it does not form a strong bond, it would likely lose its electrons to the conduction band, thus effectively behaving as a donor. X-ray spectroscopy can be used to determine the valence state of the Cr dopants, thus allowing for a determination of their environment. In Fig. 2(b) calculated spectra are shown using atomic multiplet theory in which spin-orbit and electrostatic interactions are treated on equal footing, including crystal-field interaction and charge hybridization [31]. There is good agreement with the measured data, most notably for the XMCD spectra. Fitting the XMCD spectrum by multiplet calculations, the local ground state for Cr is found as $\Psi_g = 0.7\,\Psi(d^4\underline{L}) + 0.3\,\Psi(d^3)$ in an octahedral crystal field of $10Dq = 1.5$ eV with a spin moment $m_S \approx 3\mu_B$/Cr atom, where $\underline{L}$ represents a hole state on the adjacent atoms. As mentioned in Sec. II, the energy position of the edge jump for the Cr K-edge XANES also indicated a

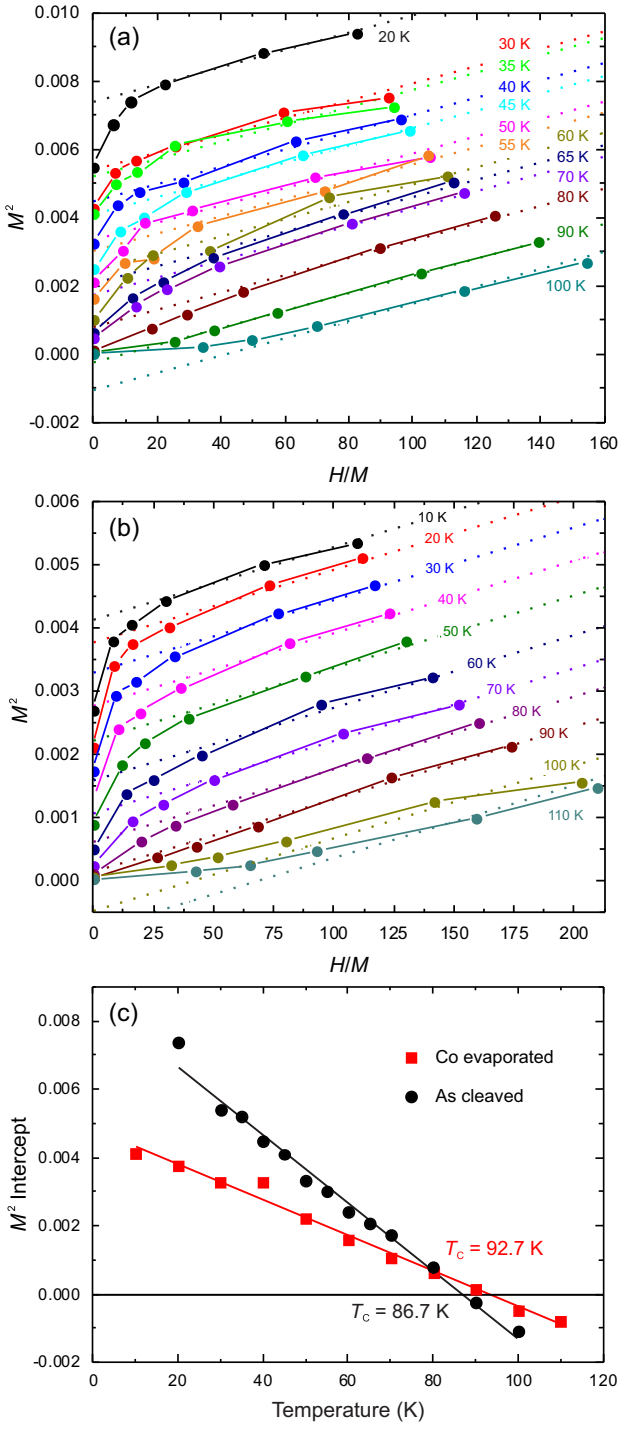

FIG. 5. Arrott plots for the Cr magnetization of (a) an as-cleaved $Cr_{0.32}Sb_{1.68}Te_3$ sample and (b) after *in situ* Co deposition. The isothermal variations of M^2 are plotted as a function of H/M, where H is the applied field and M is the magnetization as measured by the XMCD asymmetry of the Cr L_3 peak using TEY. In both plots, straight lines were fitted (shown as dotted lines) to the three data points obtained at the highest fields at each temperature. (c) The M^2 intercepts, collected from (a) and (b), are plotted against temperature. The straight lines are guides to the eye. The temperature at which the M^2 intercept goes through zero corresponds to the Curie temperature. The values for the as-cleaved (black line) and Co decorated (red line) surfaces are 86.7 K and 92.7 K, respectively. The error bars of the data points in (c) are smaller than the size of the circles and squares.

divalent Cr state. Such a nominally divalent character (Cr $d^4\underline{L}$) can be ascribed to the hybridization between the Cr $d(e_g)$ and the Te p bands, which are located just above and below the Fermi level, respectively. This result is similar as we reported for $Cr_xBi_{2-x}Se_3$ [13,16], which corresponds to a substitutional doping scenario in which Cr replaces Sb. Further indication for substitutional doping can be obtained by comparing the ionic radii. Sb^{3+} and Te^{2-} have ionic radii of 76 and 103 pm, respectively, whereas Cr^{2+} (high spin), Cr^{2+} (low spin), Cr^{3+}, Cr^{4+}, and Cr^{5+} have ionic radii of 80, 73, 61.5, 55, and 49 pm, respectively [35]. Therefore, the best-suited ion for substituting Sb^{3+} is Cr^{2+}.

Thus, similar to the case of Cr-doped Bi_2Se_3, there is a strong indication that Cr is nominally divalent when it substitutes for formally Sb^{3+} in the Sb_2Te_3 lattice. However, as in the case of the Sb-Te bond in Sb_2Te_3, which is not purely ionic but has a substantial covalent character, the Cr-Te bond also has a covalent character. The apparently isoelectronic substitution of Cr for Sb is the main reason that there is a rather weak charge carrier (hole) dependence on the Cr concentration. The strong p-d hybridization is an important indicator for determining the type of exchange coupling mechanism in a semiconductor.

B. Exchange interaction

The signs of the XMCD spectra enable us to derive the (anti)ferromagnetic coupling between the different ionic sites, which in turn might provide a clue for the ferromagnetic ordering mechanism. The Sb $M_{4,5}$ absorption (Fig. 3) corresponds to a $3d \rightarrow 5p$ transition, whereas on the other hand the Cr $L_{2,3}$ absorption corresponds to a $2p \rightarrow 3d$ transition. The interchange of the orbital quantum numbers between initial and final state in these transitions reverses the sign in the magnetic moment determination [27]. Thus the opposite signs for the XMCD at these two edges corresponds to a parallel coupling between the Sb $5p$ and Cr $3d$ moments [36].

The XMCD measurements show that the field dependence of the Sb and Cr XMCD is very similar, hence the moments couple together. Since the Sb XMCD is two orders of magnitude smaller than that of the Cr, we did not measure the full field and temperature-dependent magnetization curves for Sb.

Figures 2(a) and 4(c) show that just below the Cr L_3 edge there is an additional peak at 573.4 eV, which is not present for $Cr_xBi_{2-x}Se_3$ [16]. This photon energy corresponds to the Te M_5 absorption edge, indicating a magnetic moment residing on the Te site. The Te $M_{4,5}$ absorption corresponds to a $3d \rightarrow 5p$ transition. Therefore, since the Te M_5 and Cr L_3 XMCD have the same sign, the Te $5p$ and Cr $3d$ moments are aligned antiparallel. The relative spin orientations can be summarized as (Cr,Sb)↑-(Te)↓ and are indicated in Fig. 1.

This type of alignment is in agreement with a carrier-mediated coupling mechanism, similar to the traditional dilute magnetic semiconductor Mn-doped GaAs [19,37]. The polarized As (Te) valence holes mediate the ferromagnetic coupling between the Mn (Cr) ions in $Mn_xGa_{1-x}As$ ($Cr_xSb_{2-x}Te_3$), so that the magnetic moments induced at the Ga (Sb) and As (Te) sites couple parallel and antiparallel, respectively, with the Mn (Cr), as has been confirmed by XMCD [38]. Further

evidence for such a carrier-mediated mechanism arises from the fact that the Curie temperature is proportional to the doping concentration, as previously shown for $Cr_xSb_{2-x}Te_3$ [14].

Li *et al.* [21] reported for V-doped Sb_2Te_3 an energy shift of 0.6 eV in the V $L_{2,3}$ XAS when the sample is cooled from room temperature to $T = 10$ K, which they ascribe to the onset of ferromagnetism within the Van Vleck model. For Cr-doped Sb_2Te_3 we observe no change in the energy position of the Cr $L_{2,3}$ spectrum as a function of temperature, hence suggesting that the Van Vleck model might play no role.

Our experimental results are in agreement with those of Ye *et al.* [18] for Cr:$(Sb,Bi)_2Te_3$ and Peixoto *et al.* [22] for V:$(Bi,Sb)_2Te_3$. They agree also with the recent spin-polarized first-principles calculations by Vergeniory *et al.* [39]. These calculations showed two different exchange mechanisms determining the magnetic order in transition-metal-doped Sb_2Te_3, namely the double-exchange interaction via the Te and the indirect exchange coupling via free carriers. The strongest exchange interaction is found between magnetic moments located on different Sb planes but within the same quintuple layer (QL). This interaction occurs via a Te atom lying between two impurities and is of double-exchange type. In addition, the magnitude of the exchange coupling between adjacent atomic layers is as large as for the in-plane interaction between the nearest magnetic moments, which is an indirect exchange interaction mediated by free-carrier sp states [40]. Furthermore, these spin-polarized first-principles calculations show that the magnitude and sign of the exchange constants strongly depend on the filling of the d states. The Cr $3d$ impurity exhibits a high density of states near the Fermi level.

C. Proximity coupling

The XMCD spectra in Fig. 4 show that the moments of the deposited ferromagnetic Co layer are parallel to those of the Cr dopants. The Arrott plots measured using the Cr L_3 XMCD (Fig. 5) reveal only a modest enhancement in T_C due to proximity coupling, which is a rather unexpected result. For instance, for Fe/(Ga, Mn)As, where the Fe and Mn moments are antiparallel, a significant enhancement of the Curie temperature has been reported [41]. Also in the case of $Cr_xBi_{2-x}Se_3$ on the ferrimagnetic insulator $Y_3Fe_5O_{12}$ a large increase in T_C was found [42].

In our case the enhancement in T_C is not as large as one might expect from a magnetically doped system in proximity with a ferromagnetic material. It is easy to think of the situation where the strength of the magnetization of the Co layer would be enough to pull the Cr magnetization direction into alignment with it, thus enhancing the magnetic transition temperature. The fact that the Co layer, a good ferromagnet as demonstrated by XMCD, is not sufficient to polarize the Cr moments above T_C very significantly demonstrates the robustness of the long-range ferromagnetic order in $Cr_xSb_{2-x}Te_3$.

Referring to the spin-polarized first-principles calculations [39], in the case of Fe or Co impurities, due to an occupied minority spin-d state at the Fermi level, the magnitude of the exchange interaction increases but becomes negative because of the large exchange splitting and the narrow band character of the occupied d orbitals. Since the exchange interaction in the case of Co dopants is negative, this might similarly weaken the proximity coupling.

Unfortunately it would not be reliable to use Fe as a proximity layer, instead of Co. The Fe atoms partly penetrate into the surface and their magnetic moments are reduced due to the chemical interaction with the Te and Sb atoms of the two topmost layers [43].

Another reduction of the proximity coupling could arise from the magnetic anisotropy. Spin-polarized scanning tunneling microscopy (STM) of $Cr_{0.05}Sb_{1.95}Te_3$ showed that while the bulk bands possess an out-of-plane magnetic easy axis the topological surface state is spin polarized in the plane [44].

Since the easy axis of the Co overlayer is in-plane, while the MTI easy axis is out-of-plane, the question arises whether this would influence the T_C. However, since in the Arrott plot the value of T_C is determined from the extrapolation of the high-field magnetization, it should be insensitive to the magnetic anisotropy. While for low fields the magnetic anisotropy gives a different magnetization behavior along different magnetization directions, the magnetic anisotropy should not change the value of T_C because this value is defined in zero magnetic field, i.e., where there is no direction of the magnetic field.

V. CONCLUSION

Using soft x-ray absorption spectroscopy we determined the chemical and magnetic properties of $Cr_{0.32}Sb_{1.68}Te_3$ thin films. Comparison of the signs of the XMCD at the Cr $L_{2,3}$, Te $M_{4,5}$, and Sb $M_{4,5}$ edges shows that the Te $5p$ moment is coupled antiparallel to both the Cr $3d$ and Sb $5p$ moments. This behavior is characteristic for carrier-mediated coupling as found, e.g., in the dilute ferromagnetic semiconductor (Ga, Mn)As. Comparison of the Cr $L_{2,3}$ spectral shapes with multiplet calculations indicates a hybridized Cr state of 70% d^4 and 30% d^3 character in octahedral crystal-field symmetry. This hybridization is another indication pointing towards carrier-mediated coupling.

Arrott plots measured using the Cr L_3 XMCD show a Curie temperature of ∼87 K for the as-cleaved film. After deposition of a thin layer of ferromagnetic material in the form of Co onto the surface, T_C is raised to ∼93 K. The XAS and XMCD spectra demonstrate that the Co/MTI interface remains intact, i.e., no reaction between Co and the MTI takes place. The small enhancement of T_C due to proximity coupling means that long-range ferromagnetic order in Cr-doped Sb_2Te_3 is surprisingly robust.

Our results provide a useful starting point for developing a more precise model of Cr-doped Sb_2Te_3. They are also in agreement with recent spin-polarized first-principles calculations by Vergeniory *et al.* [39] and afford a deeper insight into the origin of magnetism in MTIs.

ACKNOWLEDGMENTS

We acknowledge XMCD beam time on ID32 at the European Synchrotron Radiation Facility (ESRF) awarded under proposal HC-2718 as well as XANES and EXAFS beam time on B18 at the Diamond Light Source under proposal SP-15702. This publication arises from research funded by the John Fell

Oxford University Press (OUP) Research Fund. L.B.D. was supported by the Science and Technology Facilities Council (STFC) and the Engineering and Physical Sciences Research Council (EPSRC) through a Doctoral Training Award.

[1] L. Fu, C. L. Kane, and E. J. Mele, Topological Insulators in Three Dimensions, Phys. Rev. Lett. **98**, 106803 (2007).

[2] B. A. Bernevig, T. L. Hughes, and S.-C. Zhang, Quantum spin Hall effect and topological phase transition in HgTe quantum wells, Science **314**, 1757 (2006).

[3] M. Z. Hasan and C. L. Kane, Colloquium: Topological insulators, Rev. Mod. Phys. **82**, 3045 (2010).

[4] Y. L. Chen, J. G. Analytis, J.-H. Chu, Z. K. Liu, S.-K. Mo, X.-L. Qi, H. J. Zhang, D. H. Lu, X. Dai, Z. Fang *et al.*, Experimental realization of a three-dimensional topological insulator, Bi_2Te_3, Science **325**, 178 (2009).

[5] P. Roushan, J. Seo, C. V. Parker, Y. S. Hor, D. Hsieh, D. Qian, A. Richardella, M. Z. Hasan, R. J. Cava, and A. Yazdani, Topological surface states protected from backscattering by chiral spin texture, Nature (London) **460**, 1106 (2009).

[6] C.-Z. Chang, J. Zhang, X. Feng, J. Shen, Z. Zhang, M. Guo, K. Li, Y. Ou, P. Wei, L.-L. Wang, Z.-Q. Ji, Y. Feng, S. Ji, X. Chen, J. Jia, X. Dai, Z. Fang, S.-C. Zhang, K. He, Y. Wang, L. Lu, X.-C. Ma, and Q.-K. Xue, Experimental observation of the quantum anomalous Hall effect in a magnetic topological insulator, Science **340**, 167 (2013).

[7] S. Qi, Z. Qiao, X. Deng, E. D. Cubuk, H. Chen, W. Zhu, E. Kaxiras, S. B. Zhang, X. Xu, and Z. Zhang, High-Temperature Quantum Anomalous Hall Effect in n-p Codoped Topological Insulators, Phys. Rev. Lett. **117**, 056804 (2016).

[8] Y. Okada, C. Dhital, W. Zhou, E. D. Huemiller, H. Lin, S. Basak, A. Bansil, Y.-B. Huang, H. Ding, Z. Wang *et al.*, Direct Observation of Broken Time-Reversal Symmetry on the Surface of a Magnetically Doped Topological Insulator, Phys. Rev. Lett. **106**, 206805 (2011).

[9] L. J. Collins-McIntyre, M. D. Watson, A. A. Baker, S. L. Zhang, A. I. Coldea, S. E. Harrison, A. Pushp, A. J. Kellock, S. S. P. Parkin, G. van der Laan *et al.*, X-ray magnetic spectroscopy of MBE-grown Mn-doped Bi_2Se_3 thin films, AIP Adv. **4**, 127136 (2014).

[10] L. J. Collins-McIntyre, S. E. Harrison, P. Schönherr, N.-J. Steinke, C. J. Kinane, T. R. Charlton, D. Alba-Veneroa, A. Pushp, A. J. Kellock, S. S. P. Parkin *et al.*, Magnetic ordering in Cr-doped Bi_2Se_3 thin films, Europhys. Lett. **107**, 57009 (2014).

[11] Y. Fan, X. Kou, P. Upadhyaya, Q. Shao, L. Pan, M. Lang, X. Che, J. Tang, M. Montazeri, K. Murata *et al.*, Electric-field control of spin-orbit torque in a magnetically doped topological insulator, Nat. Nanotechnol. **11**, 352 (2016).

[12] J. S. Dyck, P. Hájek, P. Lošt'ák, and C. Uher, Diluted magnetic semiconductors based on $Sb_{2-x}V_xTe_3$ ($0.01 \leqslant x \leqslant 0.03$), Phys. Rev. B **65**, 115212 (2002).

[13] A. I. Figueroa, G. van der Laan, L. J. Collins-McIntyre, S.-L. Zhang, A. A. Baker, S. E. Harrison, P. Schönherr, G. Cibin, and T. Hesjedal, Magnetic Cr doping of Bi_2Se_3: Evidence for divalent Cr from x-ray spectroscopy, Phys. Rev. B **90**, 134402 (2014).

[14] L. J. Collins-McIntyre, L. B. Duffy, A. Singh, N.-J. Steinke, C. J. Kinane, T. R. Charlton, A. Pushp, A. J. Kellock, S. S. P. Parkin, S. N. Holmes *et al.*, Structural, electronic, and magnetic investigation of magnetic ordering in MBE-grown $Cr_xSb_{2-x}Te_3$ thin films, Europhys. Lett. **115**, 27006 (2016).

[15] H. Ke, M. Xu-Cun, C. Xi, L. Li, W. Ya-Yu, and X. Qi-Kun, From magnetically doped topological insulator to the quantum anomalous Hall effect, Chin. Phys. B **22**, 067305 (2013).

[16] A. A. Baker, A. I. Figueroa, K. Kummer, L. J. Collins-McIntyre, T. Hesjedal, and G. van der Laan, Magnetic proximity-enhanced Curie temperature of Cr-doped Bi_2Se_3 thin films, Phys. Rev. B **92**, 094420 (2015).

[17] Z. Zhou, Y.-J. Chien, and C. Uher, Thin film dilute ferromagnetic semiconductors $Sb_{2-x}Cr_xTe_3$ with a Curie temperature up to 190 K, Phys. Rev. B **74**, 224418 (2006).

[18] M. Ye, W. Li, S. Zhu, Y. Takeda, Y. Saitoh, J. Wang, H. Pan, M. Nurmamat, K. Sumida, F. Ji, Z. Liu, H. Yang, Z. Liu, D. Shen, A. Kimura, S. Qiao, and X. Xie, Carrier-mediated ferromagnetism in the magnetic topological insulator Cr-doped $(Sb,Bi)_2Te_3$, Nat. Commun. **6**, 8913 (2015).

[19] T. Dietl, H. Ohno, F. Matsukura, J. Cibert, and D. Ferrand, Zener model description of ferromagnetism in zinc-blende magnetic semiconductors, Science **287**, 1019 (2000).

[20] R. Yu, W. Zhang, H.-J. Zhang, S.-C. Zhang, X. Dai, and Z. Fang, Quantized anomalous Hall effect in magnetic topological insulators, Science **329**, 61 (2010).

[21] M. Li, C.-Z. Chang, L. Wu, J. Tao, W. Zhao, M. H. W. Chan, J. S. Moodera, J. Li, and Y. Zhu, Experimental Verification of the Van Vleck Nature of Long-Range Ferromagnetic Order in the Vanadium-Doped Three-Dimensional Topological Insulator Sb_2Te_3, Phys. Rev. Lett. **114**, 146802 (2015).

[22] T. R. F. Peixoto, H. Bentmann, S. Schreyeck, M. Winnerlein, C. Seibel, H. Maaß, M. Al-Baidhani, K. Treiber, S. Schatz, S. Grauer, C. Gould, K. Brunner, A. Ernst, L. W. Molenkamp, and F. Reinert, Impurity states in the magnetic topological insulator $V:(Bi,Sb)_2Te_3$, Phys. Rev. B **94**, 195140 (2016).

[23] A. Arrott, Criterion for ferromagnetism from observations of magnetic isotherms, Phys. Rev. **108**, 1394 (1957).

[24] A. Roy, S. Guchhait, R. Dey, T. Pramanik, C.-C. Hsieh, A. Rai, and S. K. Banerjee, Perpendicular magnetic anisotropy and spin glass-like behavior in molecular beam epitaxy grown chromium telluride thin films, ACS Nano **9**, 3772 (2015).

[25] K. Fabian, V. P. Shcherbakov, and S. A. McEnroe, Measuring the curie temperature, Geochem. Geophys. Geosy. **14**, 947 (2012).

[26] A. I. Figueroa, L. B. Duffy, G. van der Laan, and T. Hesjedal, (unpublished).

[27] G. van der Laan and A. I. Figueroa, X-ray magnetic circular dichroism—a versatile tool to study magnetism, Coord. Chem. Rev. **277-278**, 95 (2014).

[28] J. Stöhr and H. König, Determination of Spin- and Orbital-Moment Anisotropies in Transition Metals by Angle-Dependent x-Ray Magnetic Circular Dichroism, Phys. Rev. Lett. **75**, 3748 (1995).

[29] G. van der Laan and H. A. Dürr, Magnetic anisotropy and exchange biasing in heterojunctions studied by transverse magnetic circular x-ray dichroism, Physica B **248**, 121 (1988).

[30] L. R. Shelford, T. Hesjedal, L. Collins-McIntyre, S. S. Dhesi, F. Maccherozzi, and G. van der Laan, Electronic structure of Fe and Co magnetic adatoms on Bi_2Te_3 surfaces, Phy s. Rev. B **86**, 081304(R) (2012).

[31] G. van der Laan and B. T. Thole, Strong magnetic x-ray dichroism in $2p$ absorption spectra of $3d$ transition-metal ions, Phys. Rev. B **43**, 13401 (1991).

[32] A. Arrott and J. E. Noakes, Approximate Equation of State for Nickel Near its Critical Temperature, Phys. Rev. Lett. **19**, 786 (1967).

[33] I. Yeung, R. M. Roshko, and G. Williams, Arrott-plot criterion for ferromagnetism in disordered systems, Phys. Rev. B **34**, 3456 (1986).

[34] S. N. Kaul, Static critical phenomena in ferromagnets with quenched disorder, J. Magn. Magn. Mater. **53**, 5 (1985).

[35] R. D. Shannon, Revised effective ionic radii and systematic studies of interactomic distances in halides and chalcogenides, Acta Cryst. A **32**, 751 (1976).

[36] A. Kimura, S. Suga, T. Shishidou, S. Imada, T. Muro, S. Y. Park, T. Miyahara, T. Kaneko, and T. Kanomata, Magnetic circular dichroism in the soft-x-ray absorption spectra of Mn-based magnetic intermetallic compounds, Phys. Rev. B **56**, 6021 (1997).

[37] T. Jungwirth, J. Masek, K. Y. Wang, K. W. Edmonds, M. Sawicki, M. Polini, J. Sinova, A. H. MacDonald, R. P. Campion, L. X. Zhao, N. R. S. Farley, T. K. Johal, G. van der Laan, C. T. Foxon, and B. L. Gallagher, Low-temperature magnetization of (Ga,Mn)As semiconductors, Phys. Rev. B **73**, 165205 (2006).

[38] A. A. Freeman, K. W. Edmonds, G. van der Laan, R. P. Campion, A. W. Rushforth, N. R. S. Farley, T. K. Johal, C. T. Foxon, B. L. Gallagher, A. Rogalev, and F. Wilhelm, Valence band orbital polarization in III-V ferromagnetic semiconductors, Phys. Rev. B **77**, 073304 (2008).

[39] M. G. Vergniory, M. M. Otrokov, D. Thonig, M. Hoffmann, I. V. Maznichenko, M. Geilhufe, X. Zubizarreta, S. Ostanin, A. Marmodoro, J. Henk, W. Hergert, I. Mertig, E. V. Chulkov, and A. Ernst, Exchange interaction and its tuning in magnetic binary chalcogenides, Phys. Rev. B **89**, 165202 (2014).

[40] C. Zener, Interaction between the d shells in the transition metals, Phys. Rev. **81**, 440 (1951).

[41] F. Maccherozzi, M. Sperl, G. Panaccione, J. Minár, S. Polesya, H. Ebert, U. Wurstbauer, M. Hochstrasser, G. Rossi, G. Woltersdorf, W. Wegscheider, and C. H. Back, Evidence for a Magnetic Proximity Effect up to Room Temperature at Fe/(Ga,Mn)As Interfaces, Phys. Rev. Lett. **101**, 267201 (2008).

[42] W. Q. Liu, L. He, Y. B. Xu, K. Murata, M. C. Onbasli, M. Lang, N. J. Maltby, S. Li, X. Wang, C. A. Ross, P. Bencok, G. van der Laan, R. Zhang, and K. L.Wang, Enhancing magnetic ordering in Cr-doped Bi_2Se_3 using high$-T_C$ ferrimagnetic insulator, Nano Lett. **15**, 764 (2015).

[43] F. Hajiheidari, W. Zhang, and R. Mazzarello, Effects of a magnetic monolayer on the structural and surface electronic properties of Sb_2Te_3, Phys. Rev. B **94**, 125421 (2016).

[44] F. Yang, Y. R. Song, H. Li, K. F. Zhang, X. Yao, C. Liu, D. Qian, C. L. Gao, and J.-F. Jia, Identifying Magnetic Anisotropy of the Topological Surface State of $Cr_{0.05}Sb_{1.95}Te_3$ with Spin Polarized STM, Phys. Rev. Lett. **111**, 176802 (2013).